Development and Calibration of an Enhanced Quasi-Dimensional Combustion Model for HSDI Diesel Engines

Federico Perini and Enrico Mattarelli
Department of Mechanical and Civil Engineering (DIMeC)
University of Modena and Reggio Emilia
strada Vignolese 905/B, I-41125 Modena, Italy

Abstract: *The paper describes the development and validation of a quasi-dimensional combustion model, applicable to any type of HSDI Diesel engines. In this model, the fundamental in-cylinder processes are taken into account, including turbulence, fuel injection, spray dynamics, ignition and combustion. In comparison to similar models presented in literature, a more physical description of average in-cylinder turbulence properties and their interaction with spray dynamics is introduced, as well as a detailed modeling of fuel jet wall impingement. Some experimental measures available in literature and CFD-3D simulations have been considered to calibrate the modeling parameters. These improved sub-models make results accuracy less dependent on the calibration carried out on each engine, so that the same parameters setting can be successfully applied to different combustion chamber configurations.*

The model is first applied to a small HSDI turbocharged Diesel engine. The specific calibration was supported by both experiments and simulation results, the latest being obtained from 3D-CFD analyses. Then, a different Diesel engine has been simulated, adopting the same set-up of the model parameters. For both engines, the comparison between experiments and simulation shows a very good agreement in terms of in-cylinder pressures and heat release rates, as well as of average in-cylinder turbulence properties. It is worth to mention that the two engines, have a quite different unit displacement, i.e. 312 and 697 cc, respectively.

As a conclusion, this model demonstrates to be a reliable tool for addressing the optimization of the main engine design parameters, such as injection rates and timings, combustion chamber base geometry, and so forth.

Keywords: *quasi-dimensional model, diesel combustion, multi-zone modeling, simulation, turbulence*

1 Introduction

Despite the recent progress in computer technology, that allows designers to run full 3D-CFD engine cycle simulations in a more reasonable amount of time, compared to just a few years ago, 1D-CFD tools are still mandatory, particularly in the early stage of design, when attention is focused more on fluid-dynamic fundamentals than on geometric details. This approach is particularly suitable for automatic optimization, carried out with genetic algorithms [1,2], since the limited computational time allows full generations to be simulated with a high number of individuals.

The most significant limitation of the CFD-1D approach is the need of experimental data that are generally not available, for instance the heat release curves for combustion modeling. To overcome this problem, a number of multi-zone (aka quasi-dimensional) predictive models have been developed through the years [3-18]. Research in this field is following three major directions: the first is an effort for reducing the tuning parameters required by the models, providing a more physical description of the in-cylinder processes; the second is the expansion of quasi-dimensional models capabilities towards different fuels (hydrogen, methane, and so forth), and combustion concepts (GDI, HCCI, PCCI); the third is the upgrading of existing models for a more accurate prediction of pollutant emissions, for instance introducing models for NOx and soot formation, or even coupling the model to complex chemistry solvers [19,20]. The main purpose of the multi-zone model presented in this paper is to reduce the dependence of the parameters set-up on the specific engine configuration.

While for port-fuel-injected, spark-ignited engines, some successful models have been already reported in literature [11-18], even considering gaseous fuels, a few open issues still remain on Diesel combustion [3-10]. In high speed, direct injected (HSDI) Diesel engines, combustion is strictly subsequent to droplet atomization and mixing with the surrounding air. Therefore, the modeling of these processes plays a key role in any predictive approach. Unfortunately, spray patterns are related to the specific geometry of the chamber and its own flow field, so that numerical models tend to be 'engine-dependent', in the sense that different engines require different calibrations of the tuning parameters, spoiling much of the numerical tool's effectiveness.

To overcome such a problem, in this study the authors devoted particular care to describe in-cylinder turbulence features, including the contribution of fuel injection, and the interaction between spray and chamber walls. In particular, the combustion chamber, including the piston bowl, is divided into a set of cylindrical or annular "slabs", where the internal charge motion is represented by a rigid swirl vortex, whose velocity is calculated on the base of the local angular momentum. An enhanced K-k turbulence model, based on the work of Heywood and Poulos [21] is then applied to account for the mean flow energy decay. This approach, properly

integrated with an advanced spray modeling, enables a higher degree of detail in the in-cylinder flow field prediction, with an ensuing enhancement of the description of the physical phenomena governed by micro and macro turbulence, such as heat transfer, air entrainment, etc. The relevance of this approach is demonstrated in the paper, assessing the influence of the modifications proposed by the authors. A further significant advantage of the detailed representation of the combustion chamber geometry and its own flow field is an improved modeling of spray-wall interaction. Because of its key role in the control of spray patterns and in-cylinder turbulence, also an original fuel injection sub-model has been implemented. Instantaneous fuel injection rates are calculated at any operating condition through a black-box code, requiring as input data just a standard injector characterization [8], while fuel kinetic energy is considered as a source term in the in-cylinder momentum balance.

Globally, this paper describes the development, calibration and validation of a standalone quasi-dimensional combustion model, tailored for high speed, direct injected Diesel engines. The model has been coded in MATLAB®, using a modular and flexible architecture.

As far as calibration is concerned, particular attention has been paid to spray modeling. Several experimental tests carried out in constant volume chambers have been found in literature and numerically reproduced. Therefore, the spray model parameters have been tuned in order to match the experimental data, and they haven't been modified anymore in the engine applications. Also turbulence modeling was calibrated before considering actual engine operations. In this case, CFD-3D simulations using KIVA-3V provided the reference.

Finally, the global accuracy of the proposed combustion model has been assessed considering both full and partial load operations of two different automotive Diesel engines, having a unit displacement of 312 and 697 cm^3. The validation has been carried out by comparison with experimental data for in-cylinder indicated quantities, and with results from previously validated 3D-CFD simulations [22] for turbulence characteristics. The physical soundness of the proposed approach is also demonstrated through some plots reporting the spatial distribution of some key combustion parameters, such as temperature, equivalence ratio and Sauter Mean Diameter.

In the following paragraphs, a detailed overview of the quasi-dimensional model is presented.

2 In-cylinder spray modeling

Quasi-dimensional in-cylinder modelling mainly consists in the discretization of the physical problem, not intended as a method for solving non-linear differential equations, but instead as the identification of the key areas governing fluid dynamic and thermodynamic processes, in order to determine the global features of the engine cycle. Accordingly, space is divided into a limited number of zones (usually, within the 1000-2000 range): the first, main, zone represents the whole cylinder volume, while the others are generated when liquid fuel is injected into the chamber. All of them are open thermodynamic systems, able to exchange mass and energy. Furthermore, each zone containing fuel droplets is analyzed from a dynamic point of view, considering specific injection patterns.

Three coordinate systems are adopted to analyze particle dynamics within the cylinder, as shown in figure 1. The main cylindrical coordinate system allows a particle to be tracked within the cylinder, given its radial distance ρ from the cylinder axis, its depth z (defined as the axial distance from the head gasket plane) and its orientation θ (defined as the angle formed with the injection plane containing the cylinder and the injector hole axes). Then, a second Cartesian coordinate system has the same depth z coordinate as the main one, while the x coordinate represents the radial distance projected upon the injection plane. Finally, a third, yet Cartesian coordinate system, describes the position of the particle from the point of view of an injector nozzle hole, whose axis is inclined by the angle α_n as regards the head gasket plane. This system is rotated by $(\pi - \alpha_n)$ as regards the previous system, about the axis defined by direction r, which remains unchanged. In this way, local injection paths can easily be coupled with the global in-cylinder charge dynamics.

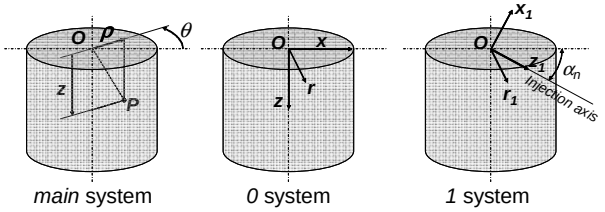

Figure 1 – Description of the coordinate systems exploited for jet particle dynamics.

SWIRL MODELING – As well known, in diffusive combustion physical fluid-dynamic processes are slower than chemical kinetics, so that they control the global combustion rate. For this reason, the influence of in-cylinder charge motion upon fuel atomization, evaporation and mixing cannot be neglected in any predictive model. Obviously, some simplifying hypotheses must be formulated, in particular about the correlation between total angular momentum and the charge motion patterns.

At the beginning of calculation (corresponding to IVC), it is assumed that the charge motion consists of one rigid vortex, so that the average angular speed of the vortex can be computed referring to the *swirl ratio* coefficient, *Rs*,:

$$\omega_{s,IVC} = Rs \cdot \omega_{eng} \,. \tag{1}$$

The global in-cylinder angular momentum is then calculated by integrating the contributions of each annular region, as shown in figure 2 and equation (2):

$$\begin{aligned} \Pi &= \iiint_{M_{cyl}} v \cdot r \, dm = \rho \iiint_{V_{cyl}} v \cdot r \, dV = \\ &= \rho H \int_0^{B/2} \omega_{s,IVC} \, r^2 \, 2\pi r \, dr = \frac{M_{cyl} \, \omega_{s,IVC} \, B^2}{8}, \end{aligned} \tag{2}$$

where r represents the radial coordinate, B the cylinder bore, H the height of the cylindrical fluid volume at IVC, V_{cyl} the total volume at IVC, and $M_{cyl} = \rho\, V_{cyl}$ the total air mass at IVC. The quantity Π is initialized by means of equation (2), then it is calculated across the engine cycle, from IVC to EVO, on the base of a simplified turbulence model described more on.

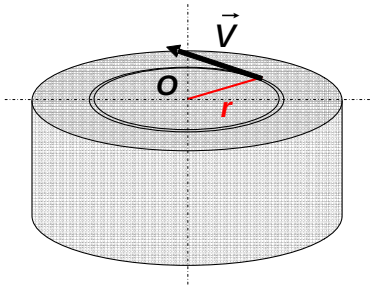

Figure 2 – Annulus of infinitesimal thickness across cylinder radius for integration of the angular momentum.

Furthermore, in order to take into account the effects due to the presence of a piston bowl, the local angular velocity ω_i of the rigid vortex along the axial direction is computed subdividing the cylinder volume into slabs, as shown in figure 3. Actually, choosing a slab height dz (by default set to be 0.10mm), the chamber volume is subdivided into a number of cylindrical (or annular, in the bowl area) slabs, applying linear interpolations upon the external surfaces which define the fluid domain. Then, for each slab, volume and internal air mass are computed. At last, the swirl rigid vortex angular velocity is computed using expression (2):

$$\Pi = \sum_i \Pi_i = \sum_{i,cyl} \frac{m_i\, \omega_i\, D_i^2}{8} + \sum_{i,ann} \frac{m_i\, \omega_i \left(D_{1,i}^2 + D_{2,i}^2\right)}{8}, \qquad (3)$$

where the two different expressions represent angular momentum values as determined for cylindrical and annular volumes ($D_{1,I}$ is the major annulus diameter, and $D_{2,I}$ is the minor one).

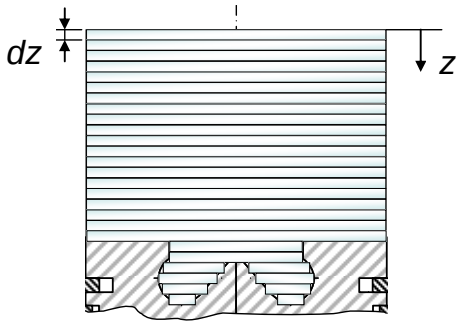

Figure 3 – Cylinder volume discretisation for applying angular momentum conservation.

From equation (3), distributing the total angular momentum by weighting it on the masses of the slabs, the angular speed of each slab becomes:

$$\omega_{i,cyl} = \frac{2\pi\,\Pi\,dz}{\rho V_i\, V_{cyl}};\quad \omega_{i,ann} = \frac{2\pi\,\Pi\,dz}{\rho V_i\, V_{cyl}} \frac{D_{1,i}^2 - D_{2,i}^2}{D_{1,i}^2 + D_{2,i}^2}. \qquad (4)$$

FUEL INJECTION: PARCELS AND ZONES – The core of the quasi-dimensional simulation model is the subdivision of the fuel spray into zones [3-5]. The fuel is injected as a liquid column, subdivided into a cluster of parcels and zones. In particular, a new parcel is generated, according to the injection law, at each timestep in which the instantaneous fuel mass-flow rate is nonzero. Each parcel is then subdivided into a fixed number of zones, distributed along the radial and circumferential jet directions, as shown in figure 4. Each zone is labelled by three indices: radial position, circumferential position, and the identification number of the parcel to which it belongs.

The injection rate is defined in terms of fuel mass-flow rate, as a function of crank angle. So, at each timestep the injected mass of the parcel is computed by integration

of the injection law, and then accordingly distributed to the zones. A total of $r_z = 5$ radial zones and $c_z = 7$ circumferential zones have been found to yield good results.

At the moment of injection, and before breakup, the characteristic speed of the jet along the injection axis, v_{ax}, is determined adopting the theory of discharge from an orifice [23]:

$$v_{ax} = C_D \sqrt{\frac{2\,\Delta p}{\rho_l}}, \qquad (5)$$

where Δp is the pressure drop across the nozzle hole, ρ_l is the liquid fuel density, and C_D is the value of the discharge coefficient.

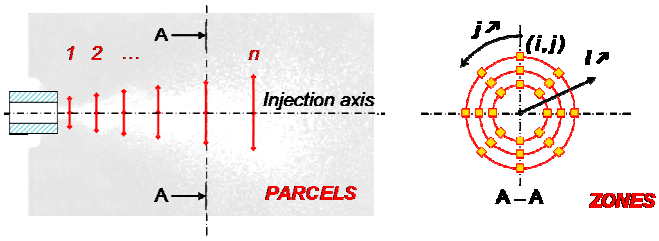

Figure 4 – Subdivision of fuel jet into parcels and zones.

The zone radial distribution is determined through the definition of the spray angle θ_{max}, which is computed following the Reitz and Bracco's correlation [24]:

$$\tan(\theta_{max}) = \frac{1}{3.0 + 0.28\,(l_n/d_n)} \cdot \frac{2\sqrt{3}}{3}\,\pi \sqrt{\frac{\rho_a}{\rho_l}}, \qquad (6)$$

where l_n and d_n, the characteristic length and diameter of the nozzle hole, define a form factor of the hole, and the ratio between air density ρ_a and liquid density ρ_l is of crucial importance. So, the radius r_{an} of the annular region defined by index i of parcel ip can be determined as follows:

$$r_{an}(i,ip) = z_1(ip) \cdot \tan\left(\frac{\theta_{max}}{2}\frac{i}{r_z}\right), \quad (7)$$

where the depth along the injection axis is given by the local parcel coordinate z_1, and the radial position of the region is defined by the ratio between the radial index and the number of radial zones. Once the radial regions have been determined, the positions of the zones in the parcel in the local injection coordinate system can be computed as:

$$\begin{pmatrix} x_1(i,j,ip) \\ r_1(i,j,ip) \\ z_1(i,j,ip) \end{pmatrix} = \int_{t_0}^{t_1} \vec{v}\, d\tau + \begin{pmatrix} r_{an}(i,ip) \cdot \cos\left(2\pi\frac{j-1}{c_z}\right) \\ r_{an}(i,ip) \cdot \sin\left(2\pi\frac{j-1}{c_z}\right) \\ 0 \end{pmatrix} \quad (8)$$

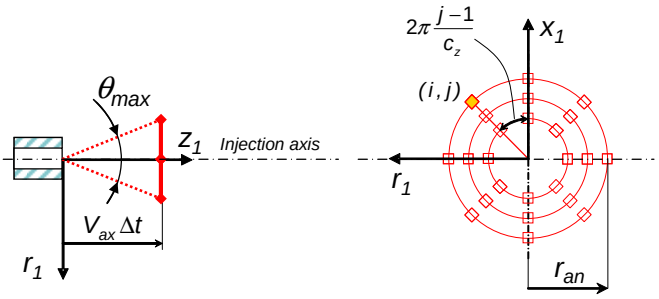

Figure 5 – Genesis of a parcel.

A schematic of the parcel genesis is represented in figure 5.

SPRAY DYNAMICS – The zone dynamics within the cylinder is affected by two phenomena: the first is the spray penetration and diffusion along and across the injection axis; the second is the dragging component given by the in-cylinder swirl motion.

In particular, the components of the velocity vector for each zone are corrected by means of a local form coefficient, given by [3]:

$$n(i) = \exp\left(-C_1\,\theta_{max}\frac{i-1}{r_z}\right); \quad (9)$$

where C_1 is a constant. The local form coefficient aims to correct the penetration velocity of the zones at the jet periphery. In this way, the components of the penetration velocity vector, under the injector local coordinate system, is:

$$\vec{v}_{inj} = \begin{pmatrix} v_{x_1}(i,j) \\ v_{r_1}(i,j) \\ v_{z_1}(i,j) \end{pmatrix} = \begin{pmatrix} v_{ax} \cdot \sin\frac{i\,\theta_{max}}{2r_z} \cdot \cos\frac{2\pi(j-1)}{c_z} \\ v_{ax} \cdot \sin\frac{i\,\theta_{max}}{2r_z} \cdot \sin\frac{2\pi(j-1)}{c_z} \\ v_{ax} \cdot \cos\frac{i\,\theta_{max}}{2r_z} \end{pmatrix}, \quad (10)$$

and then expressed in terms of the main coordinate system. Finally, the global zone velocity is given by the sum of the term due to injection and that due to in-cylinder swirling motion:

$$\vec{v} = \vec{v}_{inj} + \vec{\omega}_s \times \vec{x}, \quad (11)$$

where $\vec{x}$ represents the zone position in main system coordinates. After injection, and at each time-step, the two components of zone velocity are updated, a new velocity vector for the zone is computed, and then integrated in order to calculate the updated position of the zone within the cylinder.

FUEL BREAKUP AND EVAPORATION – The phenomenon of fuel breakup is modeled through empirical relations: the breakup time is computed following Hiroyasu's correlation [25], depending on the injection variables:

$$t_B = 4.351\frac{\rho_l\, d_n}{C_D\sqrt{\rho_a\,\Delta p}}; \quad (12)$$

after breakup time, the velocity of the spray zones decreases, as fuel droplets are fragmenting into smaller and smaller ones. So, the updated velocity component along the injection axis becomes [25]:

$$v_{ax} = 2.95\sqrt[4]{\frac{\Delta p}{\rho_a}}\sqrt{\frac{d_n}{t}}. \quad (13)$$

Since, after breakup, a zone doesn't contain a liquid fuel column anymore, but a huge number of small droplets, a characteristic Sauter Mean Diameter [26] for the droplets within the zone has to be defined. The SMD for each parcel is computed according Hiroyasu and Arai [27] model:

$$SMD = \max\{SMD_1, SMD_2\}, \quad (14)$$

where

$$\begin{aligned} SMD_1 &= 4.12\,\mathrm{Re}_{inj0}^{0.12}\,We_{inj0}^{-0.75}\left(\frac{\mu_l}{\mu_a}\right)^{0.54}\left(\frac{\rho_l}{\rho_a}\right)^{0.18}; \\ SMD_2 &= 0.38\,\mathrm{Re}_{inj0}^{0.25}\,We_{inj0}^{-0.32}\left(\frac{\mu_l}{\mu_a}\right)^{0.37}\left(\frac{\rho_l}{\rho_a}\right)^{-0.47}; \end{aligned} \quad (15)$$

the Reynolds and Weber non-dimensional groups being computed at the instant of the parcel is injected into the chamber (denoted by subscript *inj0*), and depending on the physical properties (dynamic viscosity and density) of both liquid fuel and in-cylinder air. The computed value for SMD is then distributed across the zones, according to a Gaussian distribution where the farer the zone from the axis, the smaller is its SMD, as represented in figure 6:

$$SMD(i,j) = \frac{SMD}{\sqrt{2\pi\,\sigma_d^2}} \cdot e^{-\frac{1}{2}\left(\frac{r_1(i,j)}{\sigma_d^2}\right)^2}. \quad (16)$$

Once that fuel breakup has occurred, evaporation may take place. Each zone, then, contains fuel at both liquid and gaseous phase, as well as air. Since the process of fuel evaporation involves energy exchanges between the droplets and the surrounding air, its prediction depends on the following issues.

1. Number of droplets within the zone;
2. Physical properties of the components;
3. Average physical properties of the gas mixture;
4. Non-dimensional groups for thermal, mass, motion properties of the mixture;
5. Energy balance and rate of evaporation.

As far as the number of droplets within a zone is concerned, it is assumed that all the droplets of the zone have the same SMD; then the total number of droplets is the ratio between the total liquid fuel mass within the zone and the mass of a single spherical droplet:

$$N_{DR} = \frac{m_{i,liq}}{m_d} = \frac{6\, m_{i,liq}}{\pi\, \rho_l\, SMD^3}. \tag{17}$$

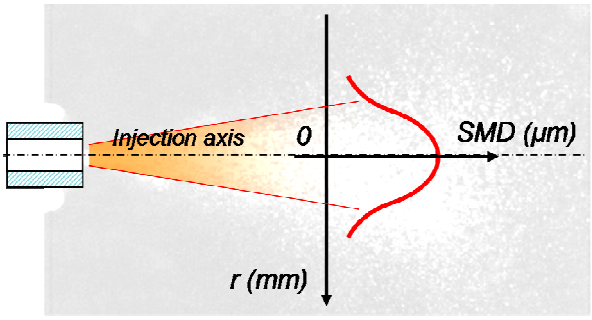

Figure 6 – Sauter Mean Diameters distribution.

The effect of a further break-up and/or coalescence is neglected [4], so that the number of droplets doesn't change anymore, while evaporation decreases their dimensions.

At each time-step, the physical properties of perfect gases have to be updated in order to predict fuel evaporation. In particular, air has been modeled as perfect dry air, while n-dodecane has been chosen as the reference fuel. The specific heat of liquids at constant pressure is computed using polynomial interpolation functions [28]:

$$c_{p,liq}(T) = c_1 + c_2 T + c_3 T^2 + c_4 T^3 + c_5 T^4, \tag{18}$$

where c_1,…c_5 are constants for each species. At the same way, the specific heat of gaseous phase fluids is computed by means of an empirical correlation found in [28]:

$$c_{p,gas}(T) = c_1 + c_2\left[\frac{c_3/T}{\sinh(c_3/T)}\right]^2 + c_4\left[\frac{c_5/T}{\sinh(c_5/T)}\right]^2. \tag{19}$$

Following a similar approach, other physical properties such as vapor tension, absolute viscosity, gas compression factor, thermal conductivity, mass diffusion coefficient, are updated for each zone at each time-step.

Then, perfect gas mixture properties, such as molar mass, viscosity, specific heat, thermal conductivity, are computed, in agreement with Dalton's law, as mole-fraction-weighted sums of the properties of the single mixture component. These properties contribute to the computation of the necessary dimensionless groups for the zones (Schmidt, Prandtl, Reynolds numbers), while Ranz and Marshall relations for evaporating droplets [29] are adopted to compute Sherwood's number for mass diffusion and Nusselt number for heat exchange:

$$\begin{aligned} Nu &= \frac{h_c\, d_l}{k_m} = 2 + 0.6 \cdot \mathrm{Re}^{1/2} \cdot \mathrm{Pr}^{1/3}; \\ Sh &= \frac{K_c\, d_l}{D_v} = 2 + 0.6 \cdot \mathrm{Re}^{1/2} \cdot \mathrm{Sc}^{1/3}; \end{aligned} \tag{20}$$

where d_l is the characteristic dimension of the droplet, i.e. the Sauter Mean Diameter of the droplets of its zone, h_c is the convective heat transfer coefficient, k_m the thermal conductivity, K_c the mass transfer coefficient and D_v the mass diffusivity.

Once the fluid mixture within a zone has been characterized in terms of physical, chemical and thermal properties, an energy balance is set for each droplet: the change in enthalpy the droplet undergoes is due to both sensible heat (convection, conduction) and latent heat (evaporation):

$$m_d \frac{dh_d}{dt} = \frac{dm_d}{dt} h_{lv} + q_d, \tag{21}$$

where the subscript d refers to the droplet, h is its enthalpy, m its mass, h_{lv} the latent heat of evaporation and q the heat transfer rate. In particular, the evaporation ratio is computed according to Borman and Johnson relation [30], as the sum of the evaporation ratios of all the droplets within the zone:

$$\begin{aligned} \frac{dm_{ev}}{dt} &= -\sum_{j=1}^{N_{DR}} \frac{dm_{d,j}}{dt} = \\ &= \pi\, d_l\, N_{DR}\, D_v\, Sh \frac{M_w\, p_t}{R\, T} \ln\left(\frac{p_t}{p_t - p_v}\right); \end{aligned} \tag{22}$$

where M_w represents the molar weight of the mixture, p_t the total pressure, p_v the vapour tension, and T the average temperature of the mixture itself. Convective heat transfer is expressed as a function of Nusselt dimensionless number [31]:

$$q = Nu\, N_{DR}\, k_m\, \pi\, d_l\, (T - T_l)\, c, \tag{23}$$

where T_l is the temperature of the liquid droplet, and c a corrective coefficient, defined according to Wakil et al. [32], which takes into account the presence of mass diffusion together with convective heat transfer:

$$c = \frac{z}{e^z - 1}, \text{ where } z = \frac{c_{p,v}\,\dot{m}_{ev}}{\pi d_l N_{DR} k_m Nu}, \qquad (24)$$

in which $c_{p,v}$ represents the fuel vapor specific heat.

Exploiting the balance (21), it is then possible to compute the change in liquid droplets' temperature within the zone:

$$\frac{dT_l}{dt} = \frac{1}{m_l c_{p,l}}\left(q - h_{lv}\,\dot{m}_{ev}\right). \qquad (25)$$

Once all these data are calculated at each time-step, liquid droplets masses, dimensions and temperatures within each zone are updated.

WALL IMPINGEMENT – Since particle impingement against the cylinder walls can significantly affect combustion performance, an improved model based on [8] has been implemented. At each timestep, the cylinder sector is modeled as a non-convex polygon, where the bowl shape is defined by the linear interpolation of a set of geometrical coordinates. As an example, a view of a sector cross section for the two chamber configurations is presented in figure 7.

Three impingement conditions have been considered, in case the parcels collisions occur: a) within the bowl; b) on the piston crown; c) against the cylinder liner (when the piston is far enough from TDC). After any wall impingement, the jet velocity law changes into [25]:

$$v_{ax} = 2.95 \sqrt[4]{\frac{t_{hit}\,\Delta p}{\rho_a}}\,\frac{d_n}{\sqrt{t}}. \qquad (26)$$

The effects on droplets distribution are also considered, following reference [33]: the normal Weber number is evaluated for checking the droplet conditions after impingement. Splash occurs whether the following condition is fulfilled:

$$We_n > 1320 \cdot La^{-0.1826}. \qquad (27)$$

The normal Weber number, We_n, and the Laplace nondimensional group, La, are defined as:

$$We_n = \frac{\rho_l\, SMD_{(i,j,ip)} \left(\vec{v}_{(i,j,ip)} \cdot \hat{n}\right)^2}{\sigma}; \quad La = \frac{\mathrm{Re}^2}{We}. \qquad (28)$$

When splash occurs, the droplets rebound from the wall and break up. Then, the new SMD of the droplets is computed under the hypothesis that the dimensions of the droplets after impingement follow a Nukiyama-Tanasawa function [34] distribution. As a result, SMD is calculated according to the following expression:

$$SMD_i = 2.16 \cdot r_m^{\frac{1}{3}} \cdot \left[30\frac{We_n}{1320\,La^{-0.1826}} - 1\right]^{\frac{1}{3}} \cdot SMD \qquad (29)$$

where r_m represents the mass fraction of broken up droplets within the impinged zone. It is computed according to [33].

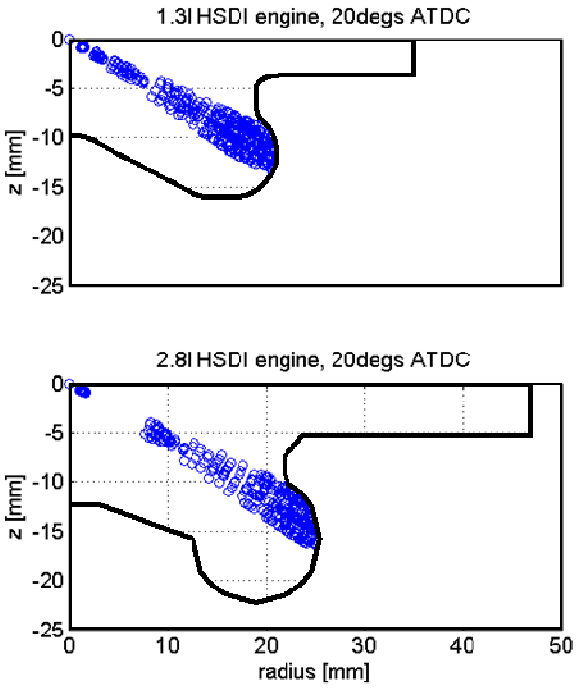

Figure 7 – View of the zones centers (blue circles) projected on the cross section of the chamber sector including the injection axis. Both engines are operated at 2000rpm, full load (the picture is taken at 20 degrees ATDC).

A fuel spray pictorial view on a sector cross section of both combustion chambers is shown in figure 7. Fuel zones are projected on the section plane, including the injector nozzle axis.

3 Combustion modeling

As far as combustion is concerned, a simplified three-step model has been adopted [4]. This approach appeared as the most suitable, since most of the physical modelling of the air/fuel mixture formation and development are based on empirical correlations. After fuel evaporation, each zone undergoes three different combustion phases:

1. Auto-ignition delay: it represents the time interval between the instant at which fuel is injected within the zone, and the instant at which combustion starts;
2. Premixed combustion phase: it is the period during which the air/fuel mixture formed during the ignition delay period burns, following a specific Arrhenius-type kinetic equation;
3. Mixing-controlled combustion phase: it represents the combustion occurring after the burning of the fuel vapor accumulated during the ignition delay period. In this case, chemical kinetics is less important, since it is the physical mixing process that limits the process development; nevertheless, kinetics can become limiting at low temperatures.

Modelling of diesel auto-ignition delay is of crucial importance in direct injected diesel engines simulation, since it affects the strength of the heat release rate within the cylinder immediately after auto-ignition, as well as pollutant formation and engine noise level. Many stationary ignition delay correlations can be found in literature, based on a variety of experiments [4,35-38]; especially, almost all of the quasi-dimensional models in literature follow an Arrhenius-type correlation by Watson et al. [35]. Instead, in this model, a newer empirical correlation, proposed by Assanis et al., [38], has been adopted. This correlation is capable of reliable predictions of ignition delay for diesel fuel also during transient load conditions. The ignition delay period has consequently been implemented by integration of the following Arrhenius-type expression, which includes dependence not only on pressure and temperature, but also on global equivalence ratio:

$$\tau = 2.40\,\phi^{-0.2}\,p^{-1.02}\,e^{\frac{2100}{T}}. \qquad (30)$$

Ignition occurs when the integral of the reciprocal of τ reaches 1 [39]:

$$\int_{t_{inj}}^{t_{ign}} \tau^{-1}\,dt = 1. \qquad (31)$$

As far as the air/fuel mixture premixed combustion is concerned, the rate of consumption of fuel vapour is computed following the Arrhenius-type kinetic equation [40]:

$$\dot{m}_b = B_1\,\rho_m^2\,x_{fv}\,x_{O_2}^5\,V\,e^{-\frac{E_c}{RT}}, \qquad (32)$$

where B_1 is the collision frequency, ρ_m is the density of the mixture, x_{fv} and x_{O2} are the mass fractions of the fuel vapour and of oxygen, respectively; V is the volume of the zone, E_c the activation energy of the reaction. This relation applies to the period after that ignition has occurred, and it is valid until all the fuel vapour evaporated during the ignition delay has burned.

For each zone in which the whole fuel vapour accumulated during the ignition delay time is over, mixing-controlled combustion is applied, and a different reaction rate expression is adopted:

$$\dot{m}_b = B_2\,m_{ev}\,p_{O_2}p^{1.5}\,e^{\frac{E_{c,2}}{RT}}, \qquad (33)$$

where again B_2 is the collision frequency, m_{ev} is the fuel vapour mass within the zone, p_{O2} is the partial pressure of oxygen within the zone, while p is the total pressure of the zone itself. Again, $E_{c,2}$ the activation energy of the reaction.

4 Turbulence

Accounting for the influence of turbulence on air-fuel mixing and combustion and wall heat transfer is of fundamental importance to analyze the operations of direct injected diesel engines, in particular to predict pollutant emissions. For this purpose, the well established, zero-dimensional energy-cascade model by Poulos and Heywood [21] has been adopted with some slight modifications. In particular, in order to avoid the necessity of entering specific values for each engine operation, initial conditions are calculated by using some empirical assumptions. The effect of fuel injection is also considered.

The core of the zero-dimensional turbulence model is a three-step energy cascade: the initial mean kinetic energy at IVC dissipates into turbulence; turbulent kinetic energy is then converted into heat by viscous dissipation. Figure 8 represents in a schematic appearance the concept of energy-cascaded transfer.

In the model, mean kinetic energy at IVC is computed from the bulk average flow velocity U, determined from swirl ratio:

$$K = \frac{1}{2}M_{cyl}\,U^2 = \frac{1}{16}M_{cyl}\left(Rs\,B\,\omega_{eng}\right)^2; \qquad (34)$$

while turbulent kinetic energy is initialised in terms of root-mean-squared turbulent velocity fluctuation, u' :

$$k = \frac{3}{2}M_{cyl}\,u'^2. \qquad (35)$$

The turbulence intensity level is defined as the ratio of the root-mean-squared turbulent fluctuation to the bulk average flow velocity:

$$u' = I\,U; \qquad (36)$$

In the present model, u' is initialised according to an empirical correlation which relates average turbulence intensity to swirl ratio for swirling flows in circular tubes [41]. Since turbulence at IVC is almost completely due to the mass flow forced into the cylinder during the intake stroke through the valve [42], turbulent dissipation is accordingly initialised assuming the diameter of the intake valve as characteristic length.

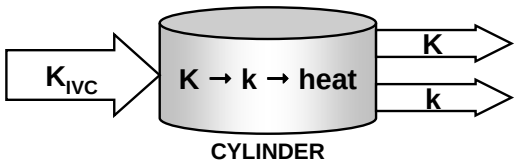

Figure 8: turbulence modelling; Mean kinetic energy K is converted into turbulent kinetic energy k and then into heat.

Then, at each time-step, the rates of change of both mean and turbulent kinetic energy are evaluated and integrated in order to update the values for K and k:

$$\frac{\partial K}{\partial t} = \frac{\partial K_{sw}}{\partial t} + \frac{\partial K_{inj}}{\partial t} - P; \qquad (37)$$

$$\frac{\partial k}{\partial t} = P - M_{cyl}\,\varepsilon - \frac{\partial K_{inj}}{\partial t}, \qquad (38)$$

where ε is turbulent kinetic energy dissipation per mass unit, K_{sw} is the amount of kinetic energy due to swirl motion within the cylinder – which is computed on the knowledge of the angular momentum – and P is the turbulent kinetic energy production term, which is assumed to be similar to turbulence production over a flat plate, and which can be expressed, in terms of turbulent viscosity μ_t, as:

$$P = \mu_t \left(\frac{\partial U}{\partial y} \right)^2 = c_\mu c_\beta \frac{K}{L_t} \left(\frac{k}{M_{cyl}} \right)^{1/2} ; \quad (39)$$

where c_μ = 0.33068 and c_β are constants, and L_t is the representative geometric length scale for the cylinder, which is assumed to be:

$$L_t = \min\left\{ \frac{B}{2} \; ; \; c_{L,1} + c_{L,2} \cdot \frac{V}{\pi B^2/4} \right\}, \quad (40)$$

where $c_{L,1}$ and $c_{L,2}$ are model constants, whose calibration is described in the following section. This formulation demonstrated to be accurate enough for Diesel engines, where the average in-cylinder flow is made up of a well structured swirl motion.

A further original feature of this turbulence model is the addition of a term that considers the influence of the huge amount of kinetic energy entering the cylinder during a high pressure injection, typically occurring in HSDI engines. More in details, a kinetic energy term has been defined as the amount of kinetic energy lost by the fuel parcels from the instant they enter the cylinder; this quantity is assumed to be converted into turbulence according to eq. (38):

$$K_{inj}(t) = \frac{1}{2} \sum_{i,j,ip} \left[m_{liq\,(i,j,ip)} + m_{ev\,(i,j,ip)} \right] \cdot \left[\left| \vec{v}_{(i,j,ip)} \right| - \left| \vec{v}_{inj\,0} \right| \right]^2 . \quad (41)$$

This term is numerically differentiated, and introduced into equation (38) for the prediction of in-cylinder mean turbulent kinetic energy.

Turbulent kinetic energy dissipation ε is approximated by:

$$\varepsilon \cong \frac{u'^3}{L_t} = \frac{\left(\frac{2k}{3M_{cyl}} \right)^{3/2}}{L_t} . \quad (42)$$

WALL HEAT TRANSFER – As far as wall cylinder heat exchange is concerned, the traditional Woschni approach [43] has been slightly modified:

$$\dot{Q}_{Wo} = c_{Wo} \, h_{Wo} \, A_{wall} \, (T - T_{wall}) , \quad (43)$$

where A_{wall} represents the instantaneous cylindrical exchange surface area, T the average gas temperature and T_{wall} the wall temperature, assumed to be constant across the whole chamber walls surface; h_{Wo} represents instead the Woschni convective-equivalent heat transfer coefficient, and c_{Wo} is a tuning parameter.

According to Woschni's approach [43], the heat transfer coefficient h_{Wo} is calculated on the basis of a bulk average velocity value, expressed as a function of the average piston speed, to account for the effects of combustion and swirl. Thanks to the enhanced turbulence model adopted in this paper, the actual charge velocity at the cylinder walls, in terms of both instantaneous swirling vortex intensity and rms turbulent fluctuation, can be entered in the calculation of the heat transfer coefficient. As a result, this approach provides a more physical and detailed description of heat transfer dependence on the instantaneous in-cylinder flow field, thus reducing the need of case by case calibration.

Furthermore, the contribution of radiating heat transfer has been added, according to [3]:

$$\dot{Q}_{rad} = \varepsilon_{app} \sigma_0 \, A_{wall} \left(T_{rad}^4 - T_{wall}^4 \right), \quad (44)$$

where the apparent grey-body emissivity, ε_{app}, has been assumed to linearly decrease during the expansion process, from its maximum value (set at 0.9) to zero; and where the apparent radiating temperature, T_{rad} , has been computed averaging the mean gas temperature and the adiabatic flame temperature, the latter obtained by assuming a slightly rich combustion, as suggested by Assanis and Heywood [3].

INFLUENCE OF THE ENHANCED TURBULENCE MODELING – Even in full 3D CFD engine simulations, the proper simulation of the interaction between turbulence and spray and combustion chemical kinetics is still a challenging task, basically because it involves time and length scales which can differ of some magnitude orders the ones from the others. In order to reduce the ensuing computational demand, turbulence models and turbulence-chemistry interaction models are widely adopted and still under development [44-45].

From a quasi-dimensional point of view, only the estimation of average in-cylinder turbulence properties is possible, while local details are neglected. However, these average values can be used to improve the prediction of fuel atomization and vaporization, air-fuel mixing and wall heat transfer. In fact, the root-mean-squared turbulent fluctuation value is added to the mean speeds calculated by the sub-models controlling air entrainment, droplet breakup, fuel evaporation and wall heat transfer.

The most important effect of this additional term can be observed on air entrainment into the spray zones. It is reminded that the traditional Hiroyasu approach assumes that spray development is related only to injection patterns, therefore turbulence has no effect on air-fuel mixing. Conversely, the new approach not only takes into account turbulence, but it provides a physical estimation of its intensity across the cycle. In Figure 9, a comparison is shown considering the same engine operating point adopted for the calibration of the combustion model (as described more in detail in the following), at four different in-cylinder average

turbulence conditions: three cases consider a constant value of *u'* across the whole engine power cycle, while the last one corresponds to the detailed turbulence modeling. As clearly visible, turbulence intensity increases the air entrainment rate in a non-linear way. Comparing the most refined approach to the standard Hiroyasu formulation (where u' is zero), the average percent variation of air entrainment is about 20%. As a conclusion, a more physical and probably more accurate description of turbulent air entrainment is achieved.

As far as wall heat transfer is concerned, its interaction with turbulence modeling is assessed at first through Figure 10, where, at the same engine operating condition of figure 9, constant values of turbulence intensities are compared to the variable value provided by the K-k turbulence model. Obviously, a greater constant turbulent fluctuation value yields a higher heat transfer rate across the whole engine power cycle. The shape of the curve does not very much when considering the instantaneous value of *u'*, computed according to the K-k turbulence model, instead of the constant values. However, it is observed that during the first 20 CA° after TDC, the K-k model is equivalent to the maximum constant turbulent intensity (10 m/s), while after this angle the proposed model copies the curve at zero turbulence.

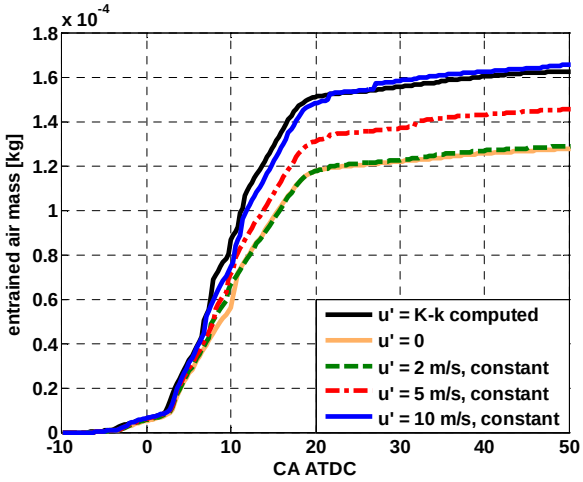

Figure 9 – Influence of turbulence modeling (in terms of instantaneous rms turbulence fluctuation, *u'*) on instantaneous air mass entrained into the spray zones: comparison among K-k computed rms turbulence, and some constant values.

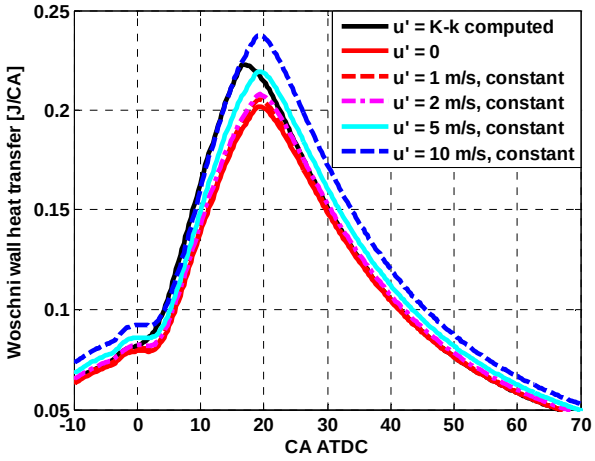

Figure 10 – Influence of turbulence modeling (in terms of instantaneous rms turbulence fluctuation, *u'*) on wall heat transfer submodel: comparison between computed rms turbulence, and some constant values.

A further influence of turbulence modeling on wall heat transfer is due to the treatment of bulk swirling motion. The K-k model allows the instantaneous swirl ratio R_s to be calculated during the cycle, as shown in Figure 11, where it is plotted at four different initialization conditions, corresponding to as many constant swirl ratios. The soundness of the proposed model is demonstrated by the shape of the curves, that are qualitatively consistent with the trends observed in CFD simulations and in experiments (for instance, see LDV measurements presented in ref. [46]).

The dissipation of the bulk swirling vortex, which is completely destroyed at about 50 crank angle degrees after TDC, strongly affects the computed wall heat transfer, as visible in Figure 12. On the one hand, it can be noticed how the peak in swirling motion, occurring around TDC, promotes the instantaneous heat transfer up to circa 45%, when compared to the constant-R_s case. On the other hand, during most of the expansion stroke, heat transfer is over-estimated without a detailed model. This latest effect can significantly condition the in-cylinder pressure trace, since, during expansion, combustion heat release can be of the same order of heat transfer rates.

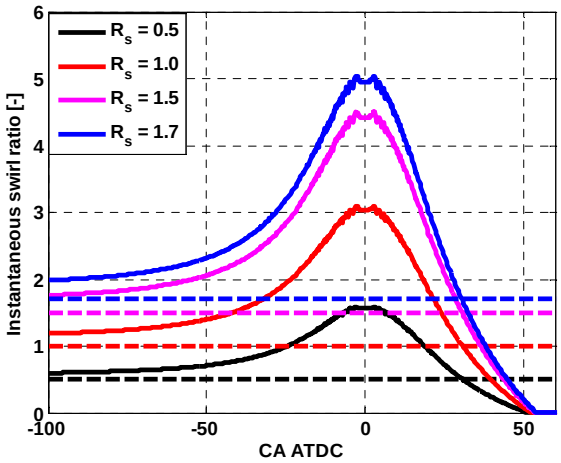

Figure 11 – Bulk instantaneous in-cylinder swirl ratio: comparison between trend calculated according to K-k turbulence model (solid lines), and constant value assumption (dotted lines), at four different initialization values of R_s.

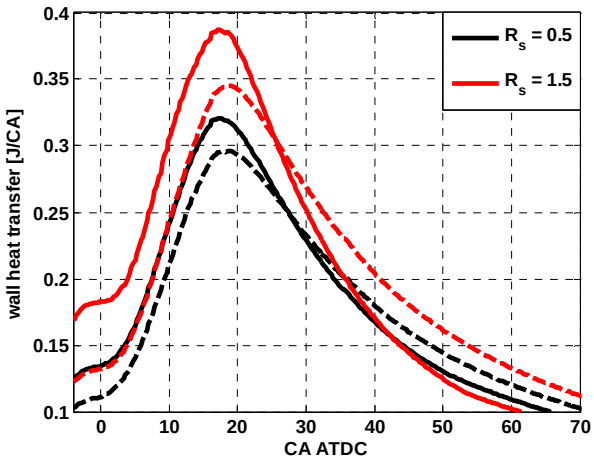

Figure 12 – Influence of swirl modeling on wall heat transfer. Comparison between constant swirl ratio (dotted lines), and K-k computed instantaneous swirl ratio (solid lines), at two different initialization R_s values.

5 Spray model calibration

Calibration of the empirical models implemented for spray dynamics has been carried out taking as a reference the detailed experimental data collected by Desantes et al. [47], for a high pressure diesel fuel injection system operating in a constant volume chamber. In particular, a unique calibration parameter C_v has been considered for correcting the spray penetration velocity defined according to eq. (13). The experimental study [46] was conducted adopting a commercial common-rail system, with a mono-orifice nozzle injector of diameter d_n= 206μm. A set of four measurements has been considered, featuring four different values of the ambient pressure, assumed to be uniform in the whole pressurized constant-volume vessel. Further details about the experimental conditions are reported, for the sake of reference, in Table 1. The comparison in terms of spray tip penetration between experimental and simulation results, the last ones obtained for a value of C_v = 1.30, is presented in figure 13. A quite good agreement can be noticed for each of the tested conditions, as the model is able to capture both trends and absolute values of spray tip penetration for the whole set of considered ambient densities. It is worth to mention that the value of the empirical constant of equation (13) was increased from 2.95 to 3.84, in order to correct some underestimation of the spray penetration observed especially at the highest ambient pressure values. This correction may be explained by the values of discharge coefficient which characterize modern common-rail injector nozzles, much higher than the 0.39 figure assumed by Hiroyasu in his work [25].

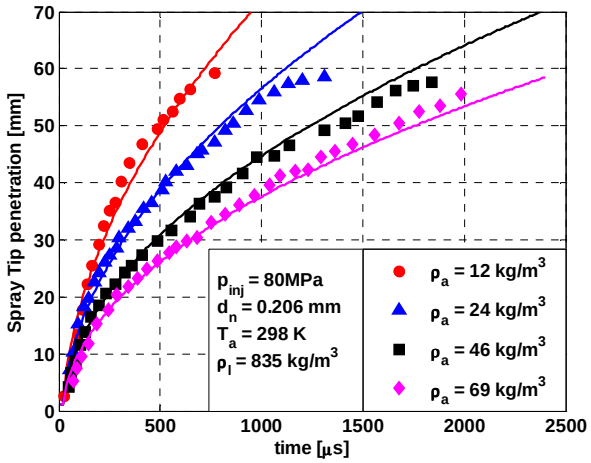

Figure 13 – Validation of the spray dynamics model against experimental data [47]. Dots represent experimental measurements, lines the simulations.

Experimental conditions for spray characterisation	
Injection system	Common-rail
Injector hole diameter [mm]	0.206
Injection pressure [MPa]	80.0
Vessel pressure [MPa]	1.0; 2.0; 4.0; 6.0
Ambient density [kg m^{-3}]	12; 24; 46; 69
Ambient temperature [K]	298
Fuel properties	
Density [kg m^{-3}]	835.0
Viscosity [kg m^{-1} s^{-1}]	$2.10 \cdot 10^{-3}$
Surface tension [kg s^{-2}]	$2.57 \cdot 10^{-2}$

Table 1 – Reference test conditions and fuel properties adopted for the spray model validation [47].

A second calibration step has then been carried out for matching the spray jet shape in terms of cone angle and axial peneteration of the transient, elliptical region located at the spray tip. The former parameter, calculated according to the Reitz and Bracco's correlation in eq. (6), has been calibrated by means of a tuning coefficient, C_θ, as it is acknowledged [4] that the model tends to under-predict the average spray angle.

The latter, i.e. the axial peneteration, is affected by the constant C_1 defined in eq. (9), which multiplies the velocity corrective term for the zones at the jet periphery. For this calibration, reference was made to the PIV measurements conducted by Cao et al. at the Yokohama University [48]. In particular, the set of data reported for injection pressures of 30, 50 and 70 MPa, was considered. The value of the tuning parameter C_v was kept constant from the previous calibration, while the best matching between these experiments and simulation was found with the setting: $C_\theta = 0.98$ and $C_1 = 1.05$. It is worth to mention that the two calibration parameters present a variation from default of less than 5%. This is the best evidence of the physical soundness and reliability of the adopted sub-models. Figure 14 presents a qualitative comparison between the numerical simulations and the experimental measurements: considering the simplified nature of the computational approach, the agreement is more than satisfactory.

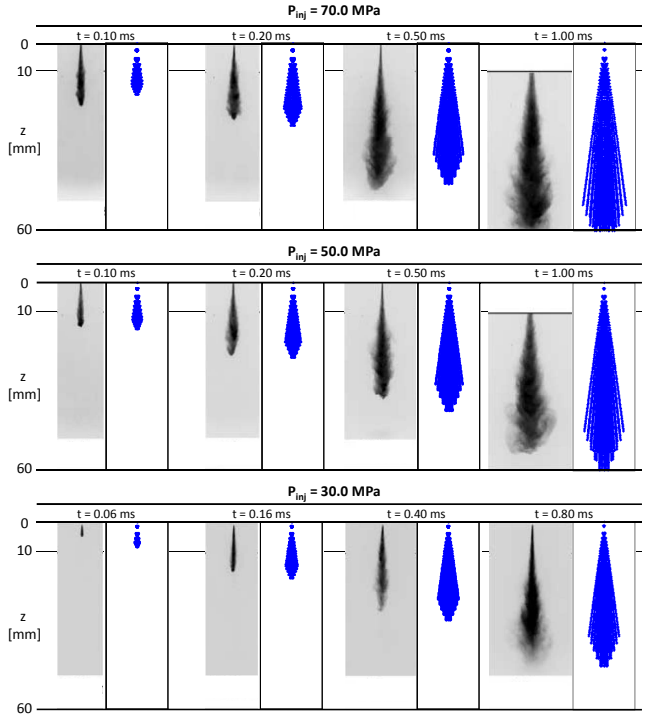

Figure 14 – Comparison between simulated and experimental visualizations of development of diesel fuel sprays injected at 30, 50 and 70 MPa [48].

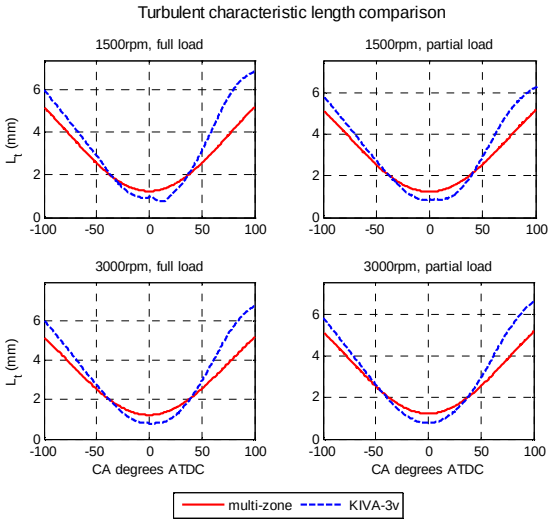

Figure 15 – Comparison between multi-zone model and 3D-CFD predicted turbulence lengths at relevant operating points.

6 Combustion model calibration

The calibration process covered 7 tuning parameters, which were defined on one reference engine operating condition.

The first two parameters, namely B_1 and B_2, define the collision frequency factors in the Arrhenius-type combustion rate equations (32) and (33), for the premixed and diffusive, phases, respectively. These two parameters strongly affect the shape of the heat release curve, and therefore represent the most important variables in the whole tuning process.

A third parameter C_τ has been considered for correcting the overall parcel ignition delay period defined in eq. (30). This coefficient may compensate some uncertainty and approximation, for instance a cetane number different from default. An increase in the value of C_τ yields a faster ignition, and thus a reduction of the premixed combustion phase, due to the lesser amount of evaporated fuel.

The two constants $c_{L,1}$ and $c_{L,2}$ respectively represent an offset value and a form factor in the definition of the integral length scale of turbulence, computed according to eq. (40). The calibration of these parameters has been performed considering their physical meaning. $c_{L,1}$ represents the minimum distance between piston crown and the engine head, thus its value is close to the chamber squish height at TDC. As far as $c_{L,2}$ is concerned, it is assumed that the characteristic length of the large scale eddies is about one half of the cylindrical-equivalent instantaneous combustion chamber height, thus a value of 0.5 has been set. The evidence of the physical soundness of these assumptions is given by the comparison with a 3D-CFD simulation, carried out applying a traditional RNG k-ε turbulence model, and plotted in Figure 15.

The last two calibration constants control the average in-cylinder turbulence properties: first of all, a tuning parameter $C_{t,inj}$ has been applied for calibrating the amount of kinetic energy converted into turbulence due to the high pressure fuel

injection, see eq. (41); secondly, a multiplier $C_{t,sw}$ has been introduced for characterizing the swirl motion induced by the intake port geometry. In the current work, the values of 0.01 and 1.4 for $C_{t,inj}$ and a $C_{t,sw}$ have been chosen in order to match the results of CFD-3D analyses, presented in the following.

In this paper, the calibration process for the combustion parameters is then reduced to the constants B_1, B_2 and C_τ. It has been carried out considering a unique operating point (2000 rpm, 100% load), for two Diesel engines of different size, whose details are summarized in the following paragraph. On both engines, the operating point is characterized by a split injection featuring one early pilot pulse (cfr. Figure 19b and 20b). The values, reported in Table 2, show that the two constants which tune premixed combustion rate and the ignition delay time remained unvaried. The unique change concerns the calibration coefficient for the computation of diffusive combustion rate, which has had to be raised by circa 2.5 times, for matching experimental pressure curves, passing from the small unit displacement engine (312 cm^3) to the larger one (697 cm^3).

Calibration (2000rpm, full load)	Engine 1	Engine 2
B_1 [m^3 kg^{-1} s^{-1}]	8.0e12	8.0e12
B_2 [s^{-1} $bar^{-2.5}$]	8.2e3	2.1e4
C_τ [-]	1.05	1.05

Table 2 – Combustion coefficients calibrated for the two different engines considered.

Figure 16 shows some three-dimensional details of fuel spray and combustion, plotted for the small engine at the reference operating point, i.e. 2000 rpm, full load. The picture demonstrates the potential of an advanced quasi-dimensional code as a tool able to get an insight of the in-cylinder phenomena. In particular, the picture presents the spatial distribution, at different crank angles, of temperature, equivalence ratio and Sauter Mean Radius.

The injection splitting does not introduce any particular problem, since the two pulses are treated in the same way and they evolve separately in the chamber. It is observed that, at this operating point, a massive wall impingement occurs, since most of the spray cloud is located near the piston bowl walls, at about 25 mm from the injector nozzle. Also the effects of the clockwise swirling motion can be noticed: the improved mixing process in the deformed spray zones leads to smaller droplets diameters and a more homogeneous spatial distribution of equivalence ratios.

This type of results, provided by the multi-zone approach, may help the designer to optimize the main combustion chamber parameters, such as compression ratio, squish height, bowl diameter and depth. Obviously, this is only the preliminary step for a more accurate, but also time-consuming, CFD multidimensional analysis.

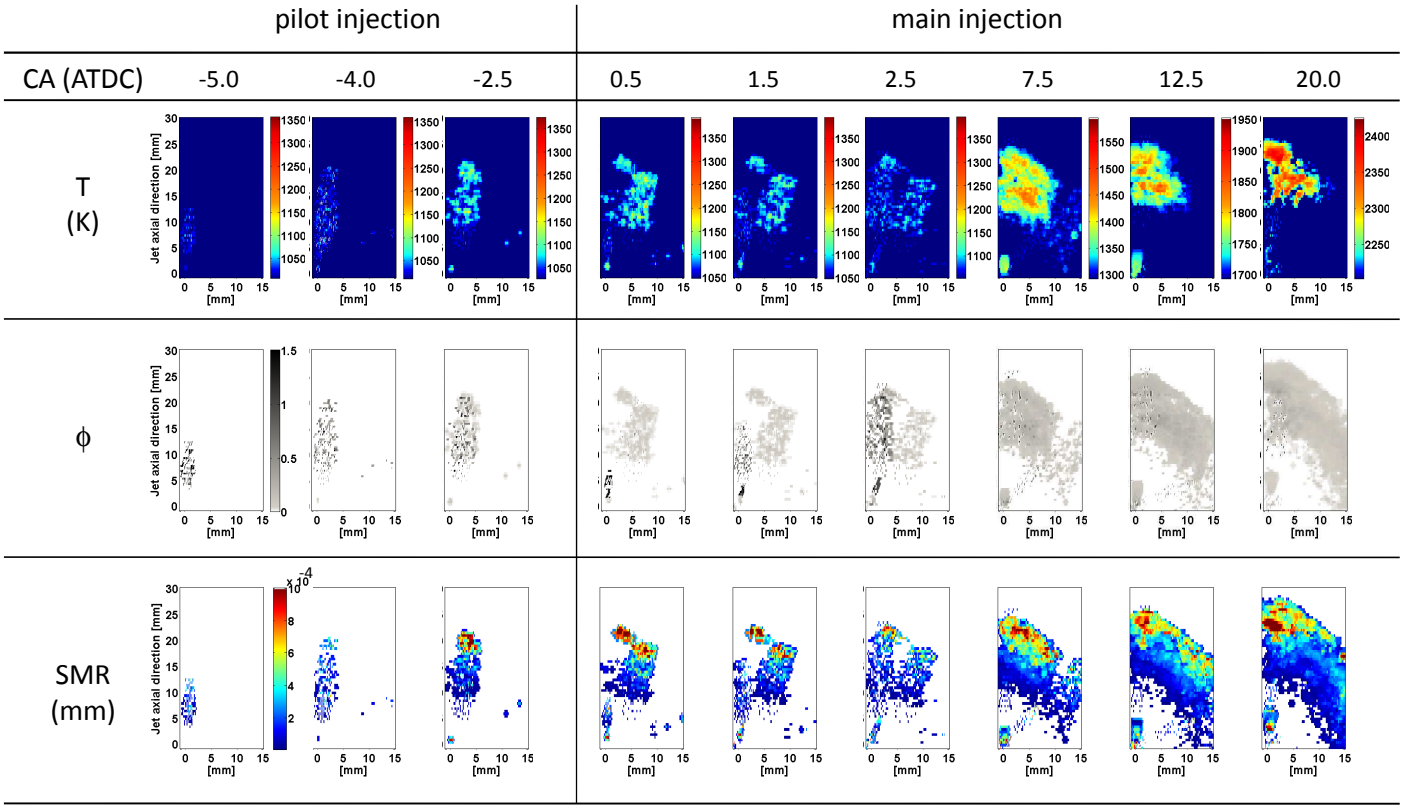

Figure 16 – Spatial distributions of gas temperature, equivalence ratio and SMR of droplets, for the same instants of time, at the calibration point on the 1.3L diesel engine (2000 rpm, 100% load).

6 Model validation on HSDI engine data

Table 3 reviews the main data for the two HSDI Diesel engines on which the model has been validated. As already mentioned, they noticeably differ in terms of unit displacement, even if the design concepts are comparable. Both engines have similar injection strategies: a unique pulse is given at full load and at high engine revs, while multiple pulses are adopted at low revs and at partial load, with one or two pre/pilot injections before the main pulse.

Fuel injection rates have been entered in the simulations by means of an empirical model, previously developed by the authors and presented in [8]. This model is based on a set of injection rate standard measures, at different pressures and energizing times, usually provided by the injector manufacturer. First, these profiles are interpolated by a set of five or two segments (depending on energizing time). Then, the main patterns of the simplified profiles are correlated to injection pressure and energizing time by a few independent parameters, which are tuned to match the experimental data. On the one hand, the accuracy of this type of model is strongly related to the amount and quality of the experimental data. On the other hand, no specific information about the injection system is required, so that this model is quite practical when results are needed in a very short time, as typically occurs in quasi-dimensional engine simulations. In the case of the engines analyzed in this paper, the injection model was supported by a comprehensive set of experimental data, covering all the operating conditions investigated in the study.

As far as the initial charge conditions are concerned, the simulation input data have been provided by a well-established 1-D CFD software (GT-Power).

The simulations have been performed for the each engine without modifications to the model calibration constants discussed in the previous paragraph, at both full and partial load. A complete set of experimental data were available for both engines, the only exception being in-cylinder pressure curves at partial load for the 1.3L engine. However, all the operating points of this engine have also been simulated by means of a customized version of KIVA-3V [49]. A review on the validation of the 3D model can be found in [22].

Table 3 – Main properties of the two HSDI diesel engines investigated.

	Engine 1	**Engine 2**
Engine type	HSDI 4-S Diesel	
Number of cylinders	4	
Total displacement [cm^3]	1248	2776
Bore [mm]	69.6	94.0
Stroke [mm]	82	100
Compression ratio	17.6:1	17.5:1
Valves per cylinder	4	
Injection system	Common-rail	
Max. Injection pressure [MPa]	160	160
Injector hole diameter [mm]	0.121	0.153
Number of injector holes	6	

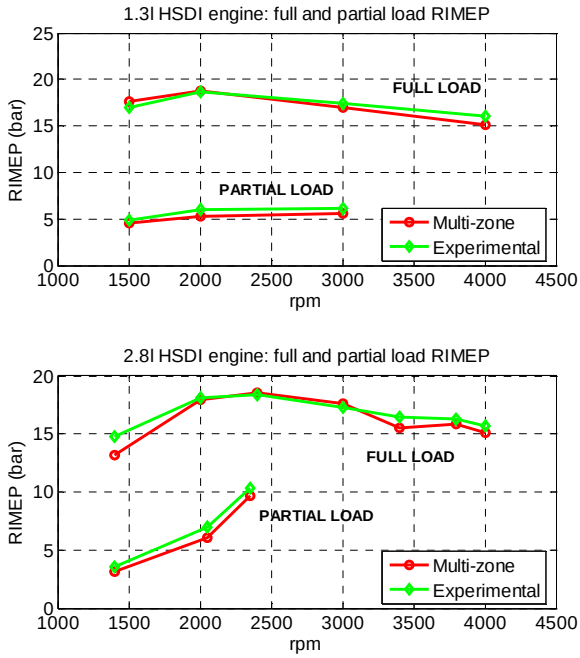

Figure 17 – Comparison between predicted and reference reduced IMEP values for the two engines considered, without any change in the model constants.

The accuracy of the proposed turbulence model is assessed through figure 18, where the results in terms of average turbulence intensity and dissipation are compared to the values provided by KIVA calculations. Considering the purpose of the quasi-dimensional model, the accuracy is more than satisfactory, the only limits arising at low speeds, where some amount of delay can be observed in the dissipation curves, and at partial loads, where the turbulence intensity peaks are slightly overestimated.

In order to compare experimental and simulation engine performance, a reduced IMEP has been defined according to:

$$RIMEP = \frac{1}{V_d}\int_{IVC}^{EVO} p\,dV \,. \qquad (45)$$

In figure 17, this parameter is shown at different loads and speeds, for both experiments and simulation. The agreement is satisfactory.

A more detailed comparison between simulation and experiments is presented in figures 19 and 20, where in-cylinder pressure and rate of heat release curves are plotted at different operating conditions. It is remarked that only pressure traces are really measured, while the combustion rates are calculated through several simplifications. In particular, the standard Rassweiler and Withrow model [42], has been applied. Therefore, the curves of combustion heat

release are intended more for a qualitative description of combustion, than for the assessment of the predictive capabilities of the simulation.

Focusing on the pressure traces, the agreement between simulation and experiments (or CFD results, for the 1.3L engine at partial load) is very good, considering that the main purpose of a quasi-dimensional combustion model is to provide consistent and reliable results in a minimum elapse of time, more than substitute full CFD calculations, which are obviously more accurate but also more time consuming. In terms of heat release curves, the less satisfactory correlation with the data derived by the experiments can be noticed in figure 20i, where the heat release rate peak is quite underestimated by the model. However, the experimental datum appears inconsistent with the other results, while the simulation output seems more reasonable.

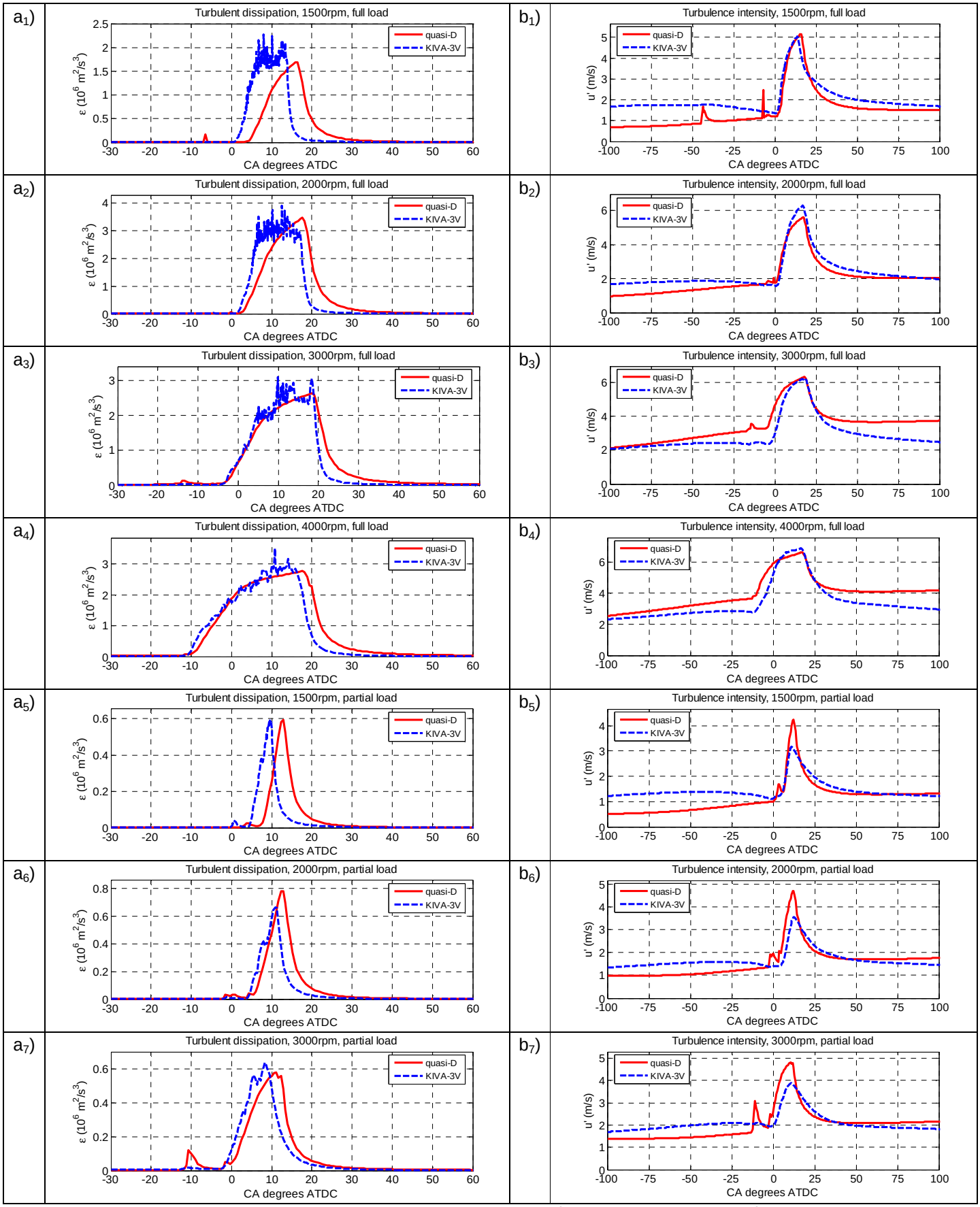

Figure 18 – Comparison between average in-cylinder turbulence properties for the 1.3l engine, at both full and partial load: turbulent dissipation ε(a) and turbulence intensity u'(b).

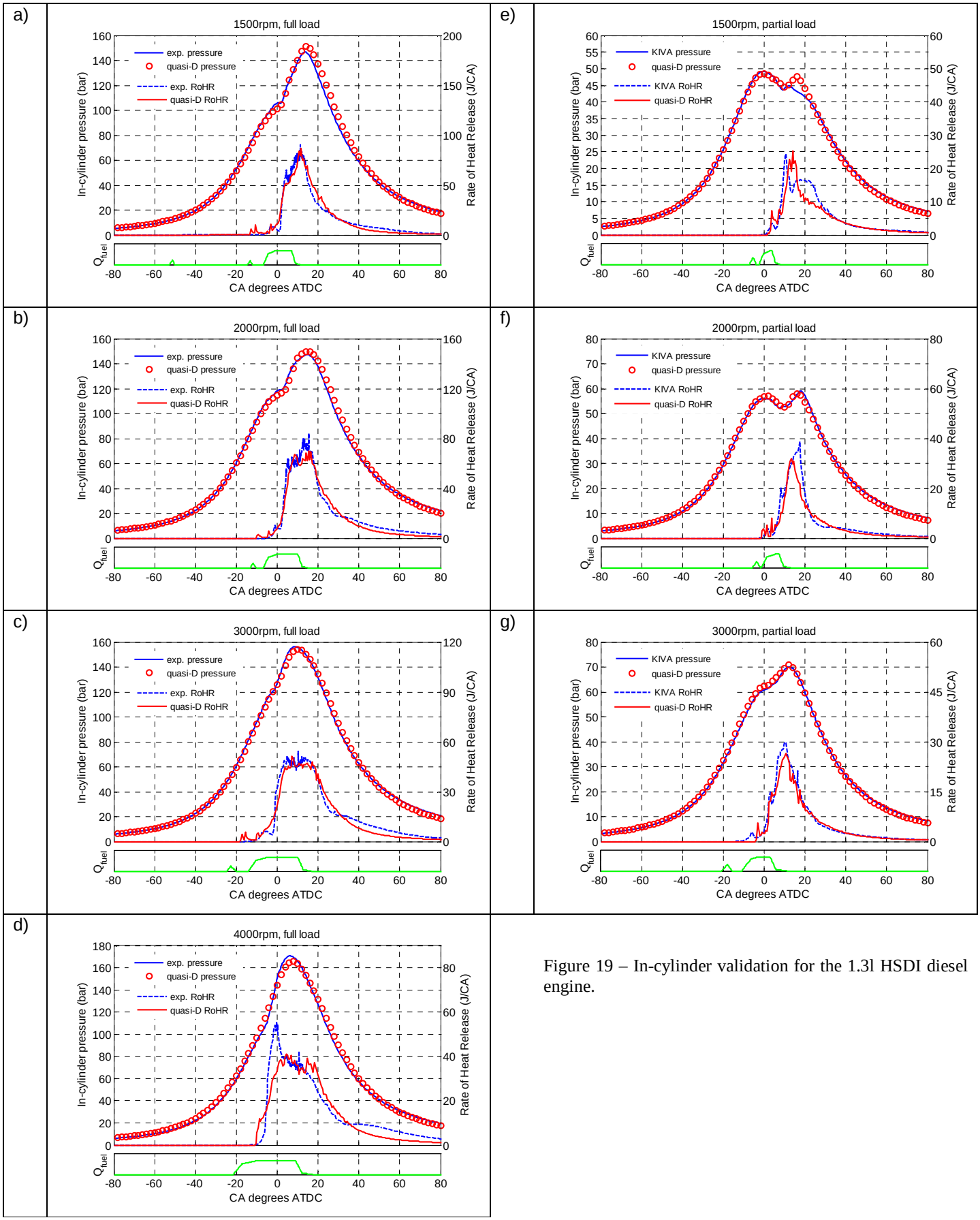

Figure 19 – In-cylinder validation for the 1.3l HSDI diesel engine.

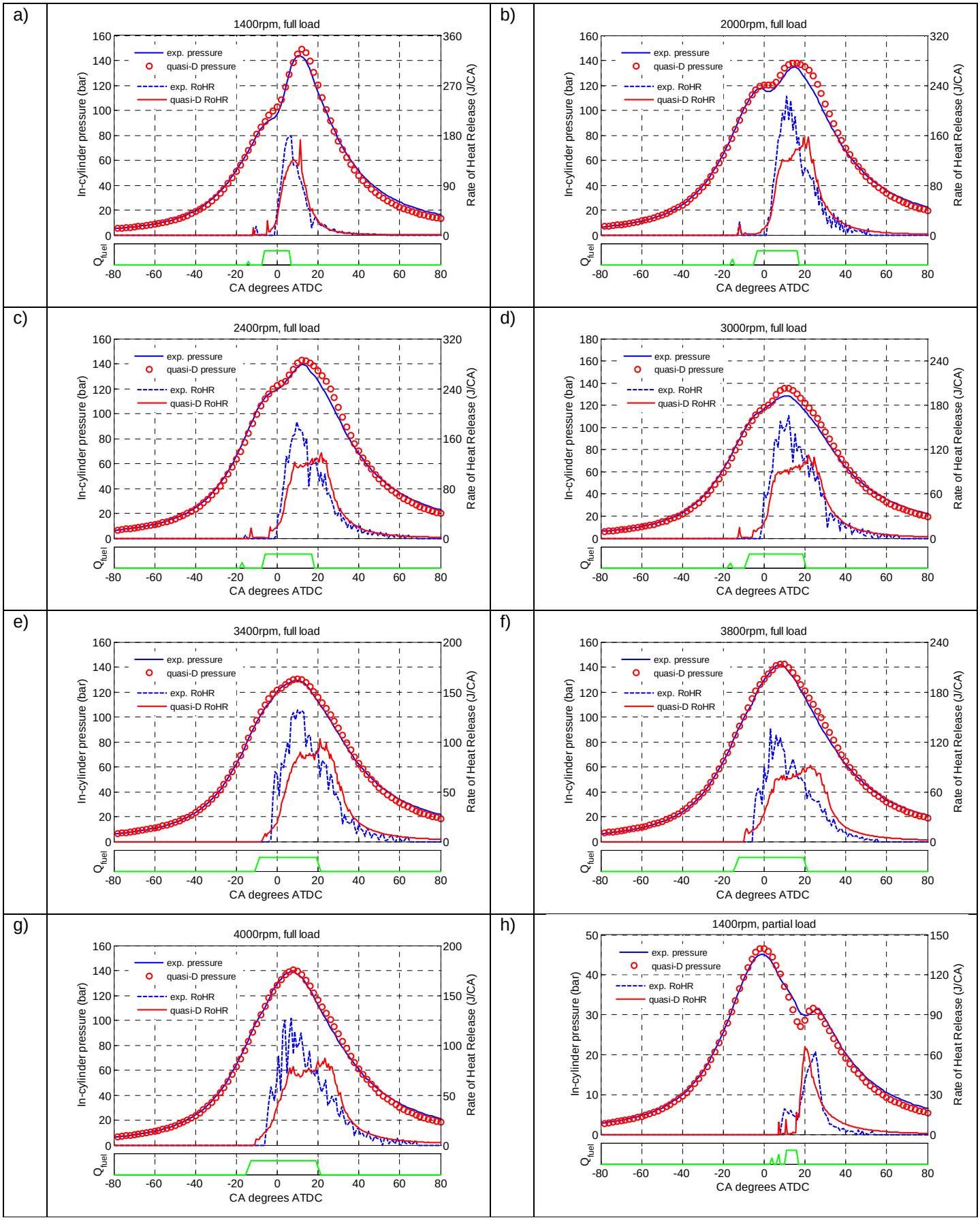

Figure 20 – In-cylinder validation for the 2.8l HSDI engine (continues on top of the next page.)

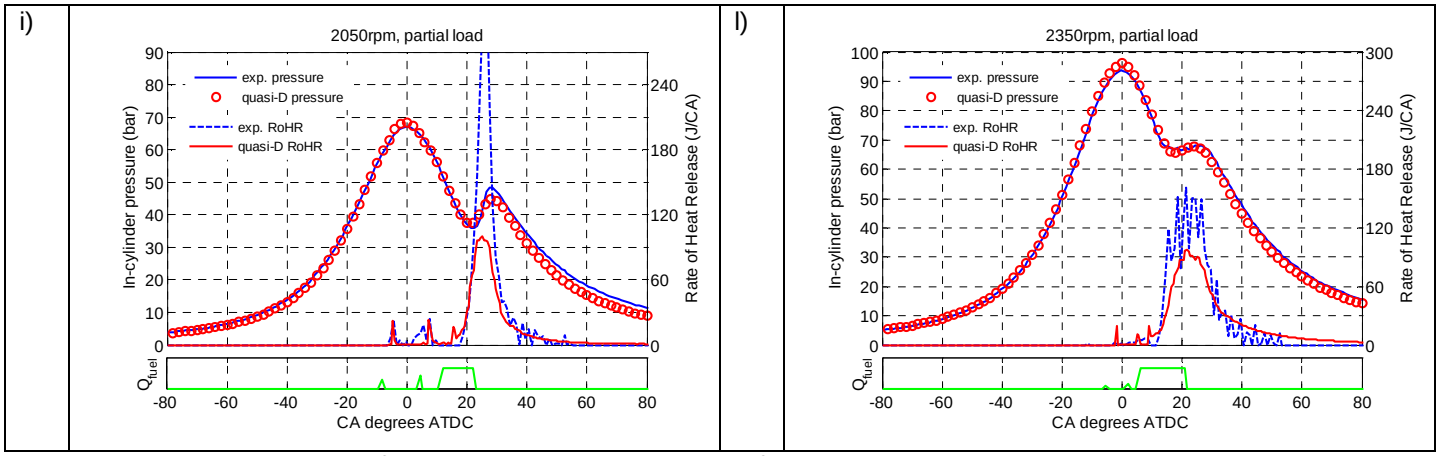

Figure 20 – In-cylinder validation for the 2.8l HSDI engine (continues from previous page.)

7 Concluding remarks

A multi-zone quasi-dimensional combustion model, for the simulation of high speed, direct injection Diesel engines has been coded, calibrated and validated by the authors.

In order to reduce the model dependence on tuning parameters, a more physical description of some fundamental in-cylinder processes has been proposed. In particular, a detailed representation of the combustion chamber geometry, through a set of cylindrical or annular "slabs", has been developed. Furthermore, a zero-dimensional, energy-cascade turbulence sub-model with some original features, and fully integrated with spray dynamics, has been implemented, taking into account the effects of high-pressure injection and swirling motion, and including an original, tuning-independent initialization procedure. The code also features an enhanced wall impingement sub-model, which takes into account the detailed piston bowl geometry.

After proper calibration of the spray submodels, carried out against detailed experimental data from constant volume test rigs, the code has been validated on both experimental and multidimensional CFD simulation data, derived from two current production HSDI Diesel engines, having a unit displacement of 312 and 697 cc, respectively. The proposed model demonstrated to provide accurate results in terms of both indicated quantities and in-cylinder thermal and fluid-dynamic parameters, with almost unchanged set-up of the model constants. Furthermore, the average turbulence properties predicted by the proposed model have been compared to 3D-CFD data. Also this comparison gives satisfactory results.

The reduced dependence on tuning constants achieved in this research activity will allow analyses to be carried out changing not only the operating parameters, such as injection law and initial conditions, but also the engine geometric parameters, such as bore, stroke, compression ratio and the bowl basic features. The enhanced spatial resolution provided by the proposed approach, may address the preliminary stage of the combustion chamber design process. Furthermore, thanks to the limited computational demand, this code appears a suitable tool for carrying on efficient engine optimization.

Further efforts are in progress for the implementation of predictive models of pollutant emissions, as well as for the expansion of the code capability to alternative fuels.

APPENDIX – ENGINE FRAMEWORK

All the computations are performed within a simplified framework which models engine cycle between IVC and EVO: basically, it includes the mass and energy conservation equations for zones and cylinder, and the modelling of in-cylinder turbulence and wall heat transfer.

MASS AND ENERGY BALANCES – Each open thermodynamic system undergoes a rate of change in its total mass which is equal to the sum of the mass flow rates into and out of itself [31]:

$$\dot{m} = \sum_k \dot{m}_k \,. \tag{46}$$

In the simplified engine framework herein implemented, intake and exhaust processes are neglected, and mass exchange only involves the main air zone, and the spray zones generated during injection. First of all, air mass rate for each spray zone is ruled by air entrainment into the zone itself, which is computed assuming conservation of the zone momentum at the instant of injection [4], and air consumption due to stoichiometric fuel combustion:

$$\dot{m}_a = \frac{-m_{i,liq} v_{inj0}}{v^2} \frac{dv}{dt} - \dot{m}_b \alpha_{st} \,. \tag{47}$$

Moreover, as far as the change in fuel vapour content in each of the zones is concerned, the two contributions due to evaporation of liquid fuel droplets and combustion have been considered:

$$\dot{m}_f = \dot{m}_{ev} - \dot{m}_b . \quad (48)$$

Finally, the rate of formation of combustion products has been computed assuming stoichiometric combustion of the fuel vapour:

$$\dot{m}_c = \dot{m}_b \cdot (1 + \alpha_{st}) . \quad (49)$$

As far as energy balance is concerned, the first law of thermodynamics has been applied to yield cylinder temperatures of the air and spray zones [3]:

$$mc_P \dot{T} = \sum_k \dot{m}_k h_k + \dot{Q} + (V - mc_T)\dot{p} - mc_\phi \dot{\phi} - \dot{m}h , \quad (50)$$

where the energy change rate is given by the sum of, respectively: the net enthalpy rate due to air entrainment, fuel evaporation, combustion products formation; the total heat transfer to the zone; the contributions due to pressure, equivalence ratio, and zone mass ratio. The heat released during combustion doesn't appear explicitly, but is embedded into the difference between enthalpies of the combustion products and of the reactants.

The thermodynamic properties of the mixture, including enthalpy and the specific heats at constant pressure, temperature, equivalence ratio, have been computed according to [50,51]:

$$h = h(T, p, \phi); \quad (51)$$

$$c_p = \left.\frac{\partial h}{\partial T}\right|_{p,\phi} ; \; c_T = \left.\frac{\partial h}{\partial p}\right|_{T,\phi} ; \; c_\phi = \left.\frac{\partial h}{\partial \phi}\right|_{p,T} . \quad (52)$$

Finally, as far as in-cylinder pressure is concerned, assuming ideal gas behaviour, as well as isentropic compression and expansion strokes, it has been assumed that [42]:

$$\dot{p} = \frac{\gamma - 1}{V}\dot{Q}_{tot} - \frac{\gamma}{\gamma - 1} p \dot{V} , \quad (53)$$

where

$$\dot{Q}_{tot} = LHV \cdot \sum_{i,j,ip} \dot{m}_b - \dot{Q}_{Wo} - \dot{Q}_{rad} , \quad (54)$$

represents the total instantaneous net heat release rate within the cylinder. Since global wall heat transfer involves the whole cylinder, in order to be able to apply the energy balance to each zone, it is then distributed, weighting its components on mass and temperatures:

$$\dot{Q} = -\dot{Q}_{rad} \frac{mT^4}{\sum_{i,j,ip} m_{(i,j,ip)} T^4_{(i,j,ip)}} - \dot{Q}_{Wo} \frac{mT}{\sum_{i,j,ip} m_{(i,j,ip)} T_{(i,j,ip)}} . \quad (55)$$

EGR – Exhaust gas recirculation has a special importance on Diesel engine operation, and thus it cannot be neglected for proper simulation. For this reason, in the model it has been considered following the definition in terms of mass percentage:

$$EGR(\%) = 100 \cdot \frac{m_{EGR}}{M_{cyl}} . \quad (56)$$

The exhaust mass m_{EGR} is then considered as a thermal capacity which doesn't interact with neither air/fuel mixing, nor combustion within each zone. Instead, it affects indirectly these processes, through partial pressures and concentrations of fuel vapour and fresh air that diminish as the amount of recycled exhaust gas increases..

NOMENCLATURE

LATIN SYMBOLS

A	Area [m^2]
B	Cylinder bore [m]
c	Corrective coefficient for thermal exchange
C_D	Discharge coefficient
C_1	Jet shape correction constant (see (9))
c_ϕ	Specific heat at constant equivalence ratio [J kg^{-1}]
c_L	Turbulence length law constant
c_p	Specific heat at constant pressure [J kg^{-1}]
c_T	Specific heat at constant temperature [J kg^{-1}]
cyl	Cylinder
c_z	Number of circumferential zones
d_n	Nozzle hole diameter [m]
$D_{1,2}$	Internal and external annulus diameters [m]
D_v	Mass diffusivity [m^2 s^{-1}]
E_c	Activation energy [J $kmol^{-1}$]
h	Enthalpy [J kg^{-1}]
h_c	Convective heat transfer coefficient [W m^{-2} K^{-1}]
h_{lv}	Latent heat of vaporization [J kg^{-1}]
h_{Wo}	Wall exchange convective coefficient [J kg^{-1} K^{-1}]
H	Height [m]
I	Turbulence intensity [%]
k	Thermal conductivity [W m^{-1} K^{-1}]
k_t	Turbulent kinetic energy [kg m^2 s^{-2}]
K	Kinetic energy [kg m^2 s^{-2}]
K_c	Mass transfer coefficient
La	Laplace number [-]
l_n	Nozzle hole internal length [m]
m	Mass [kg]
$\dot{m}$	Mass rate [kg s^{-1}]
n(i)	Local jet shape correction coefficient
N_{DR}	Number of droplets within a zone
Nu	Nusselt number [-]
M_{cyl}	Total in-cylinder mass [kg]
M_w	Molar weight [g mol^{-1}]
P	Turbulence production term [kg m^2 s^{-3}]
p	Pressure [Pa]
p_v	Vapour tension [Pa]
q	heat transfer rate [W]
$\dot{Q}$	Thermal exchange power [W]
r	Radial coordinate [m]

r_{an}	Zone coordinate along the radial jet direction [m]
r_m	Broken up droplets ratio
r_z	Number of radial zones
R	Perfect gas constant [J mol^{-1} K^{-1}]
Re	Reynolds number [-]
Rs	Swirl ratio coefficient [-]
Sh	Sherwood number [-]
t	Time [s]
t_B	Break-up time [s]
T	Absolute temperature [K]
u'	Turbulence intensity [m s^{-1}]
U	Average swirl flow velocity [m s^{-1}]
v	velocity [m s^{-1}]
V	Volume [m^3]
We	Weber number [-]

GREEK SYMBOLS

α	Air-fuel ratio [-]
ε	Turbulent kinetic energy dissipation [m^2 s^{-3}]
ε_{app}	Apparent grey-body emissivity [-]
γ	Isentropic index [-]
ω	Angular velocity [s^{-1}]
μ	Dynamic viscosity
μ_t	Turbulent viscosity
ρ	Density [kg m^{-3}]
θ_{max}	Spray angle [deg]
σ_d	Standard deviation
σ_0	Stefan-Boltzmann constant [W m^{-2} K^{-4}]
σ	Surface tension [kg s^{-2}]
$d\tau$	Time integration variable [s]
τ	Auto-ignition delay [s]
Π	Total angular momentum [kg m^2 s^{-1}]

SUBSCRIPTS

a	air
app	apparent
ax	Along the injection axis direction
b	Referring to burned fuel
c	Referring to combustion products
d	Referring to a single droplet
eng	Engine crank
f	Fuel
ev	Referring to the evaporated fuel
gas	Gaseous phase
hit	Referring to zone impingement instant
i,ann	Annular cylinder slab index
i,cyl	Fully cylindrical slab index
i	Radial zone index
ign	Ignition
inj	Injection
inj0	At the zone injection time
j	Circumferential zone index
ip	Parcel index
l	Liquid fuel phase
liq	Liquid phase
m	Gas mixture average
n	Normal direction
O_2	Oxygen
r	reference
s, sw	Swirling vortex
st	stoichiometric
t	Turbulence
tot	Referring to the global in-cylinder mass
v	Fuel vapour phase
wall	Cylinder + piston wall surface
Wo	Woschni heat transfer correlation

ZONE COORDINATES (see figure 1)

ρ, θ, z	*Main* cylindrical coordinate system
x, r, z	*0* global cartesian coordinate system
x_1,r_1,z_1	*1* local injection cartesian coordinate system

ABBREVIATIONS

ATDC	After top dead centre
BDC	Bottom Dead Centre
CA	Crank Angle
CFD	Computational fluid-dynamics
DI	Direct Injection
EGR	Exhaust gas recirculation
EVO	Exhaust valves opening
GDI	Gasoline Direct Injection
HCCI	Homogeneous charge compression ignition
HSDI	High speed direct injected diesel engine
IMEP	Indicated mean effective pressure
IVC	Intake valve closure
LHV	Lower heating value [MJ/kg]
NO_x	Nitrogen oxides
PIV	Particle Image Velocimetry
RIMEP	Reduced IMEP between $-CA_r$ and CA_r
RMSE	root mean squared error
SMD	Sauter Mean Diameter
TDC	Top Dead Centre

REFERENCES

1. T. Hiroyasu, M. Miki, M. Kim, S. Watanabe, H. Hiroyasu, H. Miao. Reduction of Heavy Duty Diesel Engine Emission and Fuel Economy with Multi-Objective Genetic Algorithm and Phenomenological Model. SAE technical paper 2004-01-0531, 2004.
2. H. Hiroyasu, H. Miao, T. Hiroyasu, M. Miki, J. Kamiura, S. Watanabe – "Genetic Algorithms Optimization of Diesel Engine Emissions and Fuel Efficiency with Air Swirl, EGR, Injection Timing and Multiple Injections". SAE technical paper 2003-01-1853, 2003.
3. D.N.Assanis, J.B.Heywood – "Development and Use of a Computer Simulation of the Turbocompounded Diesel System for Engine Performance and Component Heat Transfer Studies", SAE paper 860329, 1986.
4. D. Jung, D.N. Assanis, "Multi-Zone DI Diesel Spray Combustion Model for Cycle Simulation Studies of Engine Performance and Emissions", SAE paper 2001-01-1246.
5. H. Hiroyasu, T. Kadota, M. Arai, "Development and Use of a Spray Combustion Modeling to Predict Diesel Engine

Efficiency and Pollutant Emissions (Part 1 Combustion Modeling)", Bull. JSME 26 (1983), 569-575.
6. H. Hiroyasu, T. Kadota, M. Arai, "Development and Use of a Spray Combustion Modeling to Predict Diesel Engine Efficiency and Pollutant Emissions (Part 2 Computational Procedure and Parametric Study).
7. D.T. Hountalas, D.A. Kouremenos, E.G. Patriotis, V. Schwarz, K.B. Binder, "Using a Phenomenological Multi-Zone Model to Investigate the Effect of Injection Rate Shaping on Performance and Pollutants of a DI Heavy Duty Diesel Engine", SAE paper 2002-01-0074.
8. T.Cerri, A. Onorati, E. Mattarelli, "1D Engine Simulation of a small HSDI Diesel Engine Applying a Predictive Combustion Model", ASME Journal of Engineering for Gas Turbines an Power 130 (2008), 012802, 1-10.
9. P. Zhou, S. Zhou, D. Clelland, "A modified quasi-dimensional multi-zone combustion model for direct injection diesels", International Journal of Engine Research 7 (2006), 335 – 345.
10. E. G. Pariotis, D. T. Hountalas, C. D. Rakopoulos – "Investigating the effect of piston bowl geometry on the performance and emissions of a HSDI diesel engine using a new quasi-dimensional model of combustion". Proceedings of the 20th International Conference on Efficiency, Cost, Optimization, Simulation and Environmental Impact of Energy Systems (ECOS), ECOS07-P10, 2007.
11. S. Verhelst, C.G.W. Sheppard, "Multi-zone thermodynamic modelling of spark-ignition engine combustion - An overview", Energy Conversion and Management 50 (2009), 1326 - 1335.
12. S. Verhelst, R. Sierens, "A quasi-dimensional model for the power cycle of a hydrogen-fuelled ICE", International Journal of Hydrogen Energy 32 (2007) 3545 – 3554.
13. F.Ma, Y. Wang, M. Wang, H. Liu, J. Wang, S. Ding, S. Zhao, "Development and validation of a quasi-dimensional combustion model for SI engines fuelled by HCNG with variable hydrogen fractions", International Journal of Hydrogen Energy 33 (2008) 4863 – 4875.
14. C. D. Rakopoulos, C.N. Michos, "Quasi-dimensional, multi-zone combustion modelling of turbulent entrainment and flame stretch for a spark ignition engine fuelled with hydrogen-enriched biogas", International Journal of Vehicle Design 49 (2009), 3 – 51.
15. N.P. Komninos, D.T. Hountalas, C.D. Rakopoulos, "A parametric investigation of hydrogen hcci combustion using a multi-zone model approach", Energy Conversion and Management 48 (2007), 2934 – 2941.
16. C. Rakopoulos, C. Michos, E. Giakoumis, "Thermodynamic Analysis of SI Engine Operation on Variable Composition Biogas-Hydrogen Blends Using a Quasi-Dimensional, Multi-Zone Combustion Model", SAE paper 2009-01-0931, 2009.
17. G. D'Errico, A. Onorati, "An Integrated Simulation Model for the Prediction of Gdi Engine Cylinder Emissions and Exhaust After-Treatment System Performance", SAE paper 2004-01-0043, 2004.
18. G. D'Errico, "Prediction of the combustion process and emission dormation of a bi-fuel engine", Energy Conversion and Management 49 (2008), 3116 - 3128.
19. A. Babajimopoulos, D.N. Assanis, D.L. Flowers, S.M. Aceves, R.P. Hessel, "A fully coupled computational fluid dynamics and multi-zone model with detailed chemical kinetics for the simulation of premixed charge compression ignition engines", International Journal of Engine Research 6 (2005), 497 – 512.
20. H. Barths, C. Felsch, N. Peters. "Mixing models for the two-way-coupling of CFD codes and zero-dimensional multi-zone codes to model HCCI combustion". Combustion and Flame 156 (2009), 130-139.
21. S.G. Poulos, J.B.Heywood, "The Effect of Chamber Geometry on Spark-Ignition Engine Combustion", SAE paper 830334, 1983.
22. Montorsi, L., Rinaldini, C.A. and Golovitchev, V.I – "CFD Combustion and Emission Formation Modeling for a HSDI Diesel Engine Using Detailed Chemistry", Proceedings of the ASME Fall technical Conference, November 5-8 2006, ICE2006-1506.
23. Frank M. White. *Fluid Mechanics. 6th edition, with Student Resources CD*. McGraw Hill Higher Education, 2003. ISBN 0071215662.
24. R.D. Reitz, F.V. Bracco – "On the Dependence of Spray Angle and Other Spray Parameters on Nozzle Design and Operating Conditions", SAE technical paper 790494, 1979.
25. H. Hiroyasu, M. Arai – "Fuel Spray Penetration and Spray Angle of Diesel Engines", Trans. of JSAE, Vol. 21, pp. 5-11, 1980.
26. J. Sauter – "Determining the efficiency of Atomization by its fineness and uniformity". NACA Technical Memorandum #396, 1927.
27. H. Hiroyasu, M. Arai, M. Tabata – "Empirical Equations for the Sauter Mean Diameter of a Diesel Spray". SAE techical paper 890464, 1989
28. R. H. Perry, D. W. Green. *Perry's Chemical Engineers' Handbook*. McGraw-Hill Professional; 7th edition (1997), ISBN 0070498415.
29. W. E. Ranz, W. R. Marshall – "Evaporation from drops". Chemical Engineering Progress 48 (1952), Issue 4, pp.173-180.
30. G. L. Borman, R.J.R. Johnson – "Unsteady Vaporization Histories and Trajectories of Fuel Drops injected into Swirling Air". SAE technical paper 598C, 1962.
31. Frank P. Incropera, David P. De Witt – *Fundamentals of Heat Transfer*. John Wiley and Sons, 1981. ISBN 0-471-42711-X.
32. M.M. El Wakil, O.A. Uyehara, P.S. Myers – "A Theoretical Investigation of the Heating-up Period of Injected Fuel Droplets Vaporizing in Air", NACA Technical Note no. 3179, 1954.
33. H. Su, S. Mosbach, M. Kraft, A. Bhave, S. Kook, C. Bae – "Two-stage Fuel Direct Injection in a Diesel Fuelled HCCI Engine", SAE technical paper 2007-01-1880, 2007.
34. Z. Han, Z. Xu, and N. Trigui – "Spray/wall interaction models for multidimensional engine simulation", Int. J. Engine Research, 1(1):127–146, 2000.
35. N. Watson, A.D. Pilley, M.A.Marzouk – "Combustion Correlation for Diesel Engine Simulation". SAE technical paper 800029, 1980.

36. H. H. Wolfer, “Der Zünderzug im Dieselmotor”, VDI-Forschungscheft 392 (1938), pp. 15 – 24.
37. T. Kadota, H. Hiroyasu, H. Oya, “Spontaneous Ignition Delay of a Fuel Droplet in High Pressure High Temperature Gaseous Environments”, Bull. JSME 19 (130), 437-445, 1976.
38. D.N. Assanis, Z.S. Filipi, S.B. Fiveland, M. Syrimis, “A Predictive Ignition Delay Correlation Under Steady-State and Transient Operation of a Direct Injection Diesel Engine”, Journal of Engineering for Gas Turbines and Power 125 (2003), 450-457.
39. C.J. Livengood, C.P. Wu, “Correlation of Autoignition Phenomena in Internal Combustion Engines and Rapid Compression Machines”, Proceedings of the 5th International Symposium on Combustion, The Combustion Institute, pp. 347 – 356.
40. K. Nishida, H. Hiroyasu – “Simplified Three-Dimensional Modeling of Mixture Formation and Combustion in a D.I. Diesel Engine”. SAE technical paper 890269, 1989.
41. F. Chang, V.K. Dhir, “Turbulent flow field in tangentially injected swirl flows in tubes”, Int. J Heat and Fluid Flow 15(5), 1994; 346-356.
42. J. B. Heywood – “Internal Combustion Engine Fundamentals”, McGraw-Hill, 1988. ISBN 0-07-100499-8.
43. G. Woschni, "A Universally applicable Equation for the Instantaneous Heat Transfer Coefficient in the Internal Combustion Engine", SAE paper 670931, 1967.
44. V. I. Golovitchev, N. Nordin, R. Jarnicki, J. Chomiak, “3-D diesel spray simulations using a new detailed chemistry turbulent combustion model”, SAE paper 2000-01-1891, 2000.
45. S. Singh, R.D. Reitz, M.P.B. Musculus, “Comparison of the Characteristic Time (CTC), Representative Interactive Flamelet (RIF), and Direct Integration with Detailed Chemistry Combustion Models against Optical Diagnostic Data for Multi-Mode Combustion in a Heavy-Duty DI Diesel Engine”, SAE paper 2006-01-0055, 2006.
46. F. Payri, J. Benajes, X. Margot, A. Gil, “CFD modeling of the in-cylinder flow in direct-injection Diesel engines”, Computers & Fluids 33 (2004), 995-1021.
47. J.M. Desantes, R. Payri, F.J. Salvador, A. Gil – “Development and validation of a theoretical model for diesel spray penetration”, Fuel 85 (2006); 910 – 917.
48. Z.M. Cao, K. Nishino, S. Mizuno, K. Torii – “PIV measurement of internal structure of diesel fuel spray”, Experiments in Fluids 2000;S211-S219.
49. A.A. Amsden – “KIVA-3v: A Block-structured KIVA program for Engines with Vertical or Canted Valves”, LA-13313-MS (1997).
50. D.N.Assanis, J.E. Ekchian, R.M.Frank, J.B. Heywood – “A Computer Simulation of the Turbocharged Turbocompounded Diesel Engine System: a Description of the Thermodynamic and Heat Transfer Models”, NASA Technical Report, NASA-CR-174971, 1985.
51. R.A. Svehla, B.J. McBride, “Fortran IV Computer Program Calculations of Thermodynamic and Transport Properties of Complex Chemical Systems”, NASA TN D-7056, 1973.